Nanoscale

Accepted Manuscript

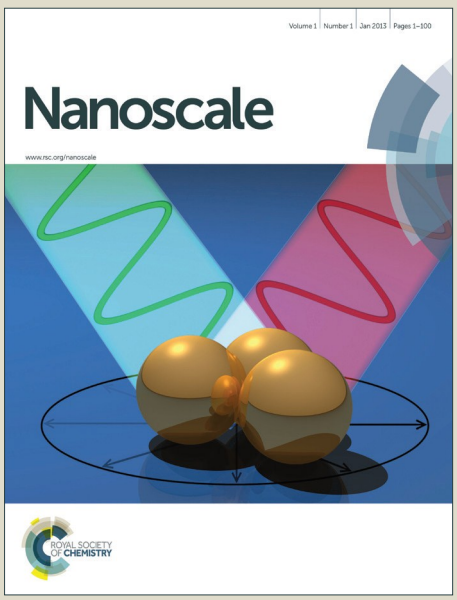

ROYAL SOCIETY OF CHEMISTRY

www.rsc.org/nanoscale

Nanoscale

ARTICLE

Wafer-scale metamaterials for polarization-insensitive and dual-band perfect absorber

Received 00th January 20xx,
Accepted 00th January 20xx

DOI: 10.1039/x0xx00000x

www.rsc.org/

Jia Liu[a], Maoxia Zhu[a], Nan Zhang[b], Haitao Zhang[a], Yu Zhou[a], Shang Sun[a], Ningbo Yi[a], Shang Gao[a], Qinghai Song[b,†], Shumin Xiao[a,*]

Mid-infrared (IR) perfect absorbers have great potentials in practical applications such as biomedical sensing and thermal energy and have been successfully demonstrated in a number of plasmonic metallic nanostructures. However, all the experimental realizations of perfect absorbers are strongly dependent on the nanofabrication techniques, which usually consume high costs and long time to fabricate a wafer scale device. Here we propose and experimentally demonstrate a wafer scale, polarization independent, wide angle, and dual-band IR perfect absorber. By fabricating double "E"-shaped metallic structures on a ZnSe coated gold film, dual-band metamaterial absorber has been uniformly realized on a 2" silicon wafer. Two absorption peaks have been realized at 18 and 27 THz, which are consistent with the designs well. We believe that our research will boost the applications of metamaterial perfect absorbers.

Introduction

Metamaterials are artificially engineered media with unique properties that have not been found in nature. [1, 2] By utilizing the novel abilities of metamaterials in tailoring and routing light, many types of fashionable phenomena have been theoretically designed and experimentally demonstrated in past decades, e.g. negative refractive index, [3, 4] electromagnetic cloak, [5, 6] superlens, [7, 8] and antennas. [9] Among these, metamaterial perfect absorber is a prominent example. The basic concept of perfect absorber is to minimize the reflectance through impedance matching and simultaneously reduce the transmittance by localizing electromagnetic waves via magnetic resonance for a longer time. Consequently, a thin metamaterial layer has been found to be able to absorb almost all the incident radiations. Such high absorption efficiency thus leads to a number of practical applications such as microbolometer, [10, 11] photodetector, [12] hyperspectral imaging, [13] and perfect absorbing layers. The initial studies on perfect absorber are focused on the microwave regions. [14] Soon after the pioneer work of Landy *et al.*, the design, fabrication, and characterization of metamaterial perfect absorber have gained considerable research attentions. The narrow single [15, 16] band has been improved to dual-band [17, 18] and finally to multiple bands. [19, 20] The dependence on polarization has also been eliminated by optimizing the nanostructures. [21-24] In past few years, due to the demands of biological sensing and chemical detection, IR metamaterial perfect absorber has been proposed and fabricated. By employing the cross pattern, X. Liu *et al.* [25] have successfully demonstrated a single band perfect absorber, which has been quickly improved to dual-band by several groups. [26, 27] Meanwhile, the angular difference and polarization dependence of metamaterial perfect absorber have also been corrected in optical regions. [28-32] Up to date, IR metamaterial absorbers have been experimentally realized in cross-patterned metamaterial, [23] elliptical nanodisks, [33] electric-field-coupled resonator, [34] and double-L-shaped metamaterials. [35] However, due to the relative small feature sizes, all these experimental demonstrations are realized using electron-beam lithography method, which usually requires much higher cost and longer time and isn't suitable for mass-fabrication. Therefore, achieving large-scale IR metamaterial absorber is the key step for their practical applications. In this research, we propose a double-E structure on a zincselenide (ZnSe) coated Au film for mid-IR metamaterial perfect absorber. Attributing to the magnetic resonances, two absorption peaks can be obtained in the mid-IR wavelength region. Most interestingly, here we experimentally fabricated the metallic structures with standard photolithography method. The similar polarization and incident angle insensitive dual-band have been obtained from different positions on the same wafer.

Numerically simulations

To realize large scale metamaterials, it is important to get a design that has minimum feature size larger than the fabrication resolution of standard photolithography (usually around 500 nm). Here we select the double-E periodically metallic structures. The unite cell of designed perfect absorber is depicted in Fig. 1(a). It is a three layer sandwich structure. The bottom layer is a 30 nm gold film, which is covered by a 600 nm ZnSe dielectric layer. The top layer is a two-dimensional periodic structure with square lattice. The period of

[a] *Integrated Nanoscience Lab, Department of Material Science and Engineering, Shenzhen Graduate School, Harbin Institute of Technology, Shenzhen, China, 518055.*
[b] *Integrated NanoscienceLab, Department of Electronic and Information Engineering, Shenzhen Graduate School, Harbin Institute of Technology, Shenzhen, China, 518055.*
* Shumin.xiao@hitsz.edu.cn, †qinghai.song@hitsz.edu.cn

unit cell is p= 9.5 μm. The detail structure within each unit is shown in Fig. 1(b), showing a connected double-E structure. The total width other geometry parameters of gold pattern are depicted in Fig. 1(b), in which w_1= 7.5 μm, w_2= 4.8 μm, w_3= 1.9 μm, and t_1= 1.15 μm. Here all the feature sizes are above 1 μm.

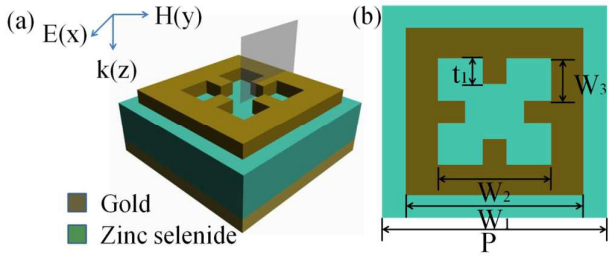

Fig.1: Schematic of our designed absorber. (a) The units cell of the structure and (b) the detailed structural information of the unit. Here we select w_1= 7.5 μm, w_2= 4.8 μm, w_3= 1.9 μm and t_1= 1.15 μm.

We then numerically calculated the absorption spectrum of the perfect absorber with a finite-element method based commercial package (COMSOL Multiphysics 4.3b). The permittivity of gold film is defined by the Drude model, $\varepsilon_m(\omega) = 1-\omega p2/\omega(\omega+i\omega c)$, where the plasmon frequency ω_p= 1.37×10^{16} Hz and the collision frequency ω_c= 4.07×10^{13} Hz. And the dielectric constant of ZnSe is 5.73. Periodic boundary conditions have been applied in both x-and y-directions to mimic the periodic structure. The transverse magnetic (TM) polarized incident electromagnetic wave direction is injected along z-axis and its electric field is along the x-axis. As the thickness of gold film is thicker than the skin depth, the transmission of incident electromagnetic waves will vanish. Consequently, the absorption intensity (A) of incident electromagnetic waves can be defined as A=1-R, where R is the reflection. Then the perfect absorption occurs where R is reduced to zero. Figure 2(a) shows the TM polarized absorption spectra of the perfect absorber in a wavelength range from 15 THz to 30 THz with normal incident light. Two absorption peaks can be clearly observed at 17.9THz and 25.6THz. The corresponding peak values are 96% and 92%, respectively, which are very close to the unity absorption. Since the structure is perfectly symmetrical, the absorption properties for TE polarized light with electric field along the y-axis is the same as result described above. Figure 2(b) shows the absorption as a function of angle of incidence under TM waves. The maximum absorption peaks for two bands remain 80% with θ up to 45°. Furthermore, the bandwidths of these two absorption peaks remain almost the same for θ smaller than 45°. To sum up, the designed metamaterial absorber displays the traits of polarization insensitivity and wide-angle incidence when θ is smaller than 45°.

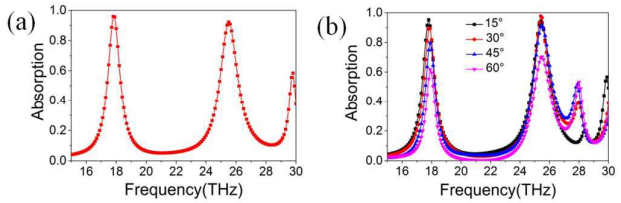

Fig. 2: (a) Absorptions spectra under normally incident TM (or TE) plane wave. (b) Absorption spectra as a function of the angle of incidence for TM (or TE) polarization plane wave.

To disclose the physical origin of the near-perfect absorptions in this dual-band metamaterial absorber, we took the cross-sectional near-field profiles plots along the grey-plane in Fig. 1(a), a plane cross the metal-dielectric-metal layers and over quarter of the unit cell. In fig. 3(a) and (b), the colour maps represent the magnetic field alongy-axis distribution (Hy) and the red arrows represent the electric displacement vectors at 17.9 THz and 25.6 THz, respectively. The electric displacement vectors in both the patterned gold layer and the ground gold plane are opposite to each other. The anti-parallel displacement vectors create circulating currents between two metal layers, resulting in an artificial magnetic moment that interacts strongly with the magnetic field of the incident light. The strong magnetic dipolar resonances that result from this interaction are then excited between the two metal layers to yield two resonant modes. The electric displacement also will result in strong confinement of the electric fields within the patterned and ground gold layer. The enhanced electric fields inside metal layers are then transformed into heat by the Ohmic losses and permit the dual-band near-perfect absorption.

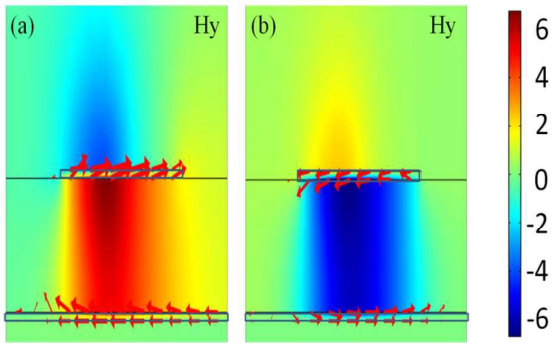

Fig. 3: The magnetic field along y-axis (Hy) distribution and the electric displacementin the grey-plane through the middle of the patterned edge at 17.9 THz and 25.6 THz illuminated under normally TM polarized incident wave.

Experiment and results

One key point of our designed double-E perfect absorber is that its minimum feature size is above 1 micron, which is the resolution limit of our mask aligner. Thus we can easily fabricate the metamaterial with standard photolithography method. Figure 4(a) illustrates the main fabrication process. The Au, ZnSe, and Au layers

are deposited onto a silicon wafer with electron-beam evaporation. The deposition rates are kept at 1Å/S. Following the initial design, the thicknesses of three layers are 30 nm, 600 nm, and 30 nm respectively. Then a 500 nm photoresist (AZ2020) is spin-coated onto the substrate and the patterns are transferred from photomask to photoresist via UV exposure and developed within AZ300 MIF. Due to the advantage of photolithography, the pattern can be easily fabricated in relative large scale. Figure 4(b) shows the picture of the whole sample on a 2" wafer. And Fig. 4(c) shows the microscope image of the transferredpattern in photoresist, where the periodic double-E shapes can be clearly observed. Then the whole sample is etched with Ar in inductively coupled plasma (ICP, Oxford ICP180) using patterned photoresist as mask.After remove the photoresist in AZ400T stripper solution, the pattern is transferred into the top gold layer. The top-view scanning electron microscope (SEM) image of the final metamaterial is shown in Fig. 4(d). Double-E shapes can be clearly observed even though their detail shapes are slightly detuned from the design.

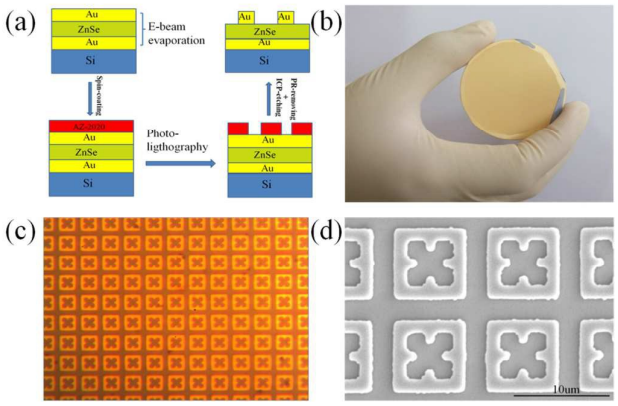

FIG.4: (a) The fabrication procedure of the metamaterial perfect absorber. (b) The picture of the whole sample. (c) The microscope image of the transfer patterns on photoresist. (d) The SEM image of the final metamaterial.

Then the mid-IR spectrum of sample is studied. Similar to the numerical calculation, the transmission T is eliminated to zero by the ground Au layer and thus the absorption can be easily obtained with A = 1- R, where R is the reflection and is recorded using Fourier transform infrared (FTIR) spectrometer (IRAffinity-1). Here, the spot size of the incident light is about 1 cm x 1 cm and the incident angle is around 30°. Figure 5 (a) shows the sample with two positions marked 1 and 2. Their corresponding absorption spectra are also shown in Fig. 5(b) and 5(c), respectively. While their positions are about 1cm away from each other, the measured absorption spectra are very similar. Both of them show two absorption peaks at 18.1 THz and 26.8 THz, respectively. These two figures further confirm the uniformity of the fabricated sample. Figure 5(d) shows the absorption spectra of TE and TM polarizations as well. While their exact values have slight difference, the main peaks and intensities are very close, clearly demonstrating the polarization insensitivity of the perfect absorber.

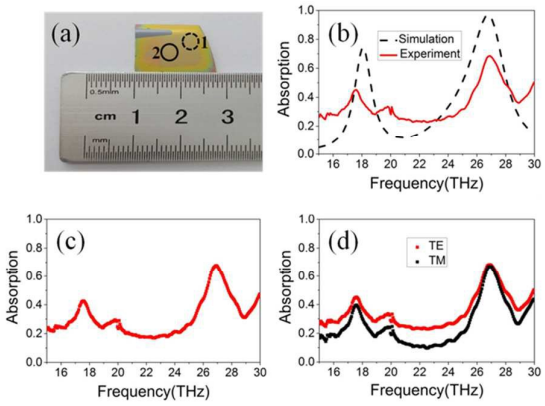

FIG.5: (a) The sample with two positions marked with 1 and 2. (b) The absorption spectra of the sample. The red solid line shows the experimental spectra of position 1 and the black dash line shows the simulation spectra by taking one unit cell of SEM image into numerical model (c) The absorption spectra of position 2.(d) The absorption spectra of position 1 under both TE and TM polarizations. The red line and the black line represent the TE and TM polarizations respectively.

The problems for the current design are the peak values of the absorptions and their frequencies. The experimentally measured peak values are only around 45% and 75% at 18.1 THz and 26.8 THz, respectively. These values are far below the initial designs in Fig. 2, especially the peak at 18.1 THz. This is mainly because of the deviations of the fabricated structures. By taking one unit cell of SEM image into numerical model, the absorption spectrum has been replotted, which is shown as dashed line in Fig. 5(b). We can see that the main trend of new calculation is similar to experimental results, where the intensity at 18.1 THz has been dramatically suppressed to 74.5 %. We note that the simulated values are still larger than the experimental results. This might have been resulted from two facts. Firstly, there is still structural deviation between double-E patterns. Secondly, there is Ar plasmon induced damage and contamination to the patterned gold structure. These problems can be eliminated by improving the photolithography and optimizing the etching recipe.

Conclusions

In conclusion, we have numerically proposed and experimentally demonstrated a dual-band perfect absorber in the infrared regime.Two perfect absorption peaks are obtained and the perfect absorber also shows good stability over a wide range of incident angle for both TE and TM polarized lights.Since the absorber is symmetrical, our designed structure also shows very nice polarization insensitivity. Most importantly, the minimum feature size is more than 1 micron and thus the wafer-scale sample has been simply realized with standard photolithography. Compared with previous reports, our research provides a cost-effective way to achieve wide-angle, polarization insensitive, dual-band absorber infrared absorbers. We believe this research will be important for the applications of infrared perfect absorber.

Acknowledgements

This work is supported by NSFC11204055, NSFC61222507, NSFC11374078, Shenzhen Peacock plan under the Nos. KQCX2012080709143322 and KQCX20130627094615410, and Shenzhen Fundamental research projects under the Nos. JCYJ20140417172417110, JCYJ20140417172417096.

Notes and references

1 N. I. Landy, S. Sajuyigbe, J. J. Mock, D. R. Smith, W. J. Padilla, *Phys. Rev. Lett.*,2008, **100(20)**, 1586-1594.
2 C. M. Watts, X. Liu, W. J. Padilla, *Adv. Mater.*, 2012, **24(23)**, OP98-120, OP181.
3 D. R. Smith, W. J. Padilla , D. C. Vier, S. C. Nemat-Nasser, S. Schultz, *Phys. Rev .Lett.*, 2000, **84(18)**, 4184-4187.
4 S. Liu, C. J. Chuang, C. W. See, G. Zoriniants, W.L. Barnes, M.G. Somekh, *Opt. Lett.*, 2009, **34**, 1255.
5 J. B. Pendry, D. Schurig, D. R. Smith, *Science*, **312(5781)**, 1780-1782.
6 D. Schurig, J. J. Mock, B. J. Justice, S. A. Cummer, J. B. Pendry, A. F. Starr, D. R. Smith, *Science*, 2006, **314(5801)**, 977-980.
7 J. B. Pendry, *Rev. Lett.*, 2000, **85(18)**, 3966-3969.
8 N. Fang, H. Lee, C. Sun, X. Zhang, *Science*, **308(5721)**, 534-537.
9 D. Dregely, R. Taubert, J. Dorfmüller, R. Vogelgesang, K. Kern, H. Giessen, *Nat. Commun.*, 2011, **2(1)**, 1 - 2.
10 P. D. Mauskopf, J. J. Bock, H. Del Castillo, W. L. Holzapfel, A. E. Lange, *Appl. Optics*, 1997, **36(4)**, 765-771.
11 A. D. Parsons, D. J.Pedder, *J .Vac. Sci. Technol. B.,* 1988, **6(3)**, 1686-1689.
12 S. Pillai, K. R. Catchpole, T. Trupke, M. A. Green, *J. Appl. Phys.*, 2007, **101(9)**, 093105.
13 B. P. Rand, P. Peumans, S. R. Forrest, *J. Appl. Phys.*, 2004, **96(12)**, 7519-7526.
14 N. I. Landy, S. Sajuyigbe, J. J. Mock, D. R. Smith, W. J. Padilla, *Phys. Rev. Lett*, 2008, **100(20)**, 1586-1594.
15 H. Tao, C. M. Bingham , A. C. Strikwerda, D. Pilon, D. Shrekenhamer, N. I. Landy, K. Fan, X. Zhang, W. J. Padilla, R. D. Averitt, *Phys. Rev. B.*, 2008, **78(24)**, 241103.
16 J. Grant, Y. Ma, S. Saha, L. B. Lok, A. Khalid, D. R. S. Cumming, *Opt. Lett.*, 2011, **36(8)**, 1524-6.
17 Y. Ma, Q. Chen, J. Grant, S. C. Saha, A. Khalid, D. R. Cumming, *Opt. Lett.*, 2011, **36(6)**, 945-947.
18 H. Tao, C. M. Bingham, D. Pilon, K. Fan, A. C. Strikwerda, D. Shrekenhamer, W. J. Padilla, X. Zhang, R. D. Averitt, *J. Phys. D. Appl. Phys.*, 2010, **43(22)**, 225102.
19 Y. Q. Ye, Y. Jin, S. He, *JOSA B*, 2010, **27(3)**, 498-504.
20 J. Grant, M. Yong, S. Saha, A. Khalid, R. S. David, Cumming, *Opt. Lett.*, 2011, **36(17)**, 3476-8.
21 F. Hu, L. Wang, B. Quan, X. Xu, Z. Li, Z. Wu, X. Pan, *J. Phys. D. Appl. Phys.*,2013,**46(19)**, 195103.
22 J. Zhu, Z. Ma, W. Sun, F. Ding, Q. He, L. Zhou, Y. Ma, *Appl. Phys. Lett.*, 2014,**105(2)**, 021102.
23 Z. Su, J. Yin, X. Zhao, *Opt. Express.*, 2015, **23(2)**, 1679-1690.
24 X. Shen, Y. Yang, Y. Zang, J. Gu, J. Han, W. Zhang, T. J. Cui, *Appl. Phys. Lett.*, 2012, **101(15)**, 154102.
25 X. Liu, T, Starr, A. F. Starr, W. J. Padilla, *Phys. Rev. Lett.*, 2010,**104(20)**, 207403.
26 K. Chen, R. Adato, H. Altug, *Acs Nano*, 2012, **6(9)**, 7998-8006.
27 Z. H. Jiang, S. Yun, F. Toor, D. H. Werner, T. S. Mayer, *Acs Nano*, 2011, **5(6)**, 4641-4647.
28 K. Aydin, V. E. Ferry, R. M. Briggs, H. A. Atwater, *Nat. Commun.*, 2011, **2**, 193-198.
29 B. Wang, T. Koschny, C. M. Soukoulis, *Phys. Rev. B.*, 2009, **80(3)**, 033108.
30 Y. Ma, Q. Chen, J. Grant, S. C. Saha, A. Khalid, D. R. *Opt. Lett.*, 2011, **36(6)**, 945-947.
31 X. Shen, T. J. Cui, J. Zhao, H. F. Ma, W. X. Jiang, H. Li, *Opt. Express*, 2011,**19(10)**, 9401-9407.
32 O. Luukkonen, F. Costa, C. R. Simovski, A. Monorchio, S. A. Tretyakov, *IEEE. T. Antenn. Propag.*, 2009, **57(10)**, 3119-3125.
33 B. Zhang, Y. Zhao, Q. Hao, B. Kiraly, *Opt. Express.*, 2011, **19(16)**, 15221-15228.
34 H. Tao , N. I. Landy,C. M. Bingham ,X. Zhang , R. D. Averitt ,W. J. Padilla , *Opt. Express.*, 2008, **16(10)**, 7181-7188.
35 Y. Bai, L. Zhao, D. Ju, Y. Jiang, L. Liu, *Opt. Express.*, 2015, **23(7)**, 8670-8680.